Exchange-correlation potentials for multiorbital quantum dots subject to generic density-density interactions and Hund's rule coupling

Nahual Sobrino,[1,2] Stefan Kurth [●],[2,3,1] and David Jacob [●][2,3,*]

[1]*Donostia International Physics Center (DIPC), Paseo Manuel de Lardizabal 4, E-20018 San Sebastián, Spain*
[2]*Nano-Bio Spectroscopy Group and European Theoretical Spectroscopy Facility (ETSF), Dpto. de Física de Materiales,
Universidad del País Vasco UPV/EHU, Av. Tolosa 72, E-20018 San Sebastián, Spain*
[3]*IKERBASQUE, Basque Foundation for Science, Maria Diaz de Haro 3, E-48013 Bilbao, Spain*

By reverse engineering from exact solutions, we obtain Hartree-exchange-correlation (Hxc) potentials for a double quantum dot subject to generic density-density interactions and Hund's rule coupling. We find ubiquitous step structures of the Hxc potentials that can be understood and derived from an analysis of stability diagrams. We further show that a generic Hxc potential can be decomposed into four basic potentials which allows for a straightforward parametrization and paves the road for the construction of Hxc potentials for interacting multiorbital systems. Finally, we employ our parametrization of the Hxc potential in density functional theory calculations of multiorbital quantum dots and find excellent agreement with exact many-body calculations.

I. INTRODUCTION

Density functional theory (DFT) is one of the most successful and popular approaches for computing the electronic structure of molecules and solids [1–3]. Its success is largely owed to its relative simplicity as well as its low computational cost as compared to other quantum many-body approaches. While DFT is an, in principle, exact theory for computing the ground-state energy and density of a many-electron system, in practice, approximations have to be made to the exchange-correlation (xc) part of the total energy functional. The most popular approximations are the local-density [2] and generalized-gradient approximations [4–7] in condensed-matter physics, and the so-called hybrid functionals in chemistry [8,9]. While these approximations usually work quite well for systems with weak to moderate electronic interactions, they completely fail for so-called strongly correlated systems where the interactions between electrons dominate over the kinetic energy. Since DFT is a formally exact theory which is valid also in the strongly correlated regime, this failure has to be assigned to shortcomings of the approximations used. Apparently, the crucial ingredient missing in standard functionals is the so-called derivative discontinuity [10], i.e., the discontinuous jump of the exact xc potential of an open system as the particle number crosses an integer [11,12]. In strongly correlated systems, the derivative discontinuity contributes a substantial part, e.g., to the fundamental gap [13] or plays a crucial role in the binding and dissociation of molecules [10].

The essential physics of strongly correlated systems can already be captured by simple but highly nontrivial lattice models such as the Anderson [14] or the Hubbard model [15],

which can be solved by advanced many-body methods as for example dynamical mean-field theory (DMFT) [16]. One way around the problems of the standard approximations of DFT is then to combine DFT with advanced many-body calculations of lattice models. In these approaches, the model Hamiltonian describes the strongly interacting part of the system, while the weakly to moderately interacting part is still described at the level of DFT. An important example is the combination of DFT with DMFT (DFT+DMFT) [17]. Originally established for the description of bulk materials, more recently the DFT+DMFT approach has been applied to the description of nanoscale systems [18] and molecules [19]. However, this approach is hampered by the so-called double-counting problem [20], limiting its predictivity. More recently, however, new efforts in combining DFT with lattice models avoiding the double-counting problem [21–23] or to solve the double-counting problem in DFT+DMFT [24] have been undertaken.

Lattice models can also be solved by a lattice version of DFT, an idea which has been pioneered by Schönhammer *et al.* [25,26]. Later this approach was further extended to study lattice problems not only in equilibrium [27–35] but also in out-of-equilibrium situations such as external time-dependent driving fields [36–42] or (steady-state) transport [43–45]. A common theme in many of these studies is again the crucial role of the derivative discontinuity (or, alternatively, step features in the xc potential) in the correct description of strongly correlated systems. For instance, for the Hubbard model, the derivative discontinuity is the only contribution to the band gap, i.e., the mechanism responsible for opening the Mott-Hubbard gap within DFT [27].

Here, in the same framework of lattice DFT, we aim for a better understanding of the structure of the (equilibrium) xc potentials of small multiorbital models. This is motivated by earlier studies on the single-impurity Anderson

*david.jacob@ehu.es

model [43–45], i.e., a single interacting impurity in contact with noninteracting leads. There it was shown that the Kondo effect, one of the hallmarks of strong correlation in the context of electron transport, can be described at the DFT level if the corresponding xc potential exhibits a step at integer particle number on the impurity. This step is already present in the xc potential of an isolated impurity in contact with a particle and heat bath described via the grand canonical ensemble [43]. The exact xc potential of the impurity connected to leads has the same qualitative features as the uncontacted one with the quantitative difference that the broadening of the step is determined (at low temperature) by the coupling to the leads while in the uncontacted case it is determined by the temperature of the bath. Therefore, we expect that knowledge of the xc potential of multiorbital models in equilibrium, apart from being interesting in itself, have a direct relevance in the context of transport.

To this end, we extensively study a double quantum dot (DQD) subject to generic interactions as the simplest possible model system for a strongly correlated multiorbital system. Using reverse engineering, we construct the exact xc potentials whose essential features are step structures which depend on the particular choice of the interaction. We illustrate how these step structures can be inferred from an analysis of the stability diagram, i.e., regions of different ground states in the parameter space given by the single-particle level structure. Analysis of the reverse-engineered xc potentials reveals that they can be constructed from four basic building blocks which can be rationalized by a corresponding decomposition of the electron-electron interaction. It is exactly this decomposition of the interaction and the corresponding xc potentials which then allows us to build xc functionals for multiorbital quantum dots (QDs) with more than two orbitals.

II. MODEL

We consider a multiorbital QD with $\mathcal{M}$ orbitals subject to direct Coulomb repulsion and Hund's rule coupling. The corresponding Hamiltonian reads

$$\mathcal{H} = \sum_\alpha v_\alpha \hat{n}_\alpha + \sum_\alpha U_\alpha \, \hat{n}_{\alpha\uparrow}\hat{n}_{\alpha\downarrow} + \sum_{\alpha<\beta} U_{\alpha\beta} \, \hat{n}_\alpha \hat{n}_\beta$$
$$- \sum_{\alpha<\beta,\sigma} J_{\alpha\beta} \, [\hat{n}_{\alpha\sigma}\hat{n}_{\beta\sigma} + (c^\dagger_{\alpha\sigma} c_{\alpha\bar\sigma} \, c^\dagger_{\beta\bar\sigma} c_{\beta\sigma})], \qquad (1)$$

where $c_{\alpha\sigma}$ ($c^\dagger_{\alpha\sigma}$) are the annihilation (creation) operators for orbital α and spin σ, $\hat{n}_{\alpha\sigma}$ is the corresponding number operator and $\hat{n}_\alpha = \hat{n}_{\alpha\uparrow} + \hat{n}_{\alpha\downarrow}$. U_α is the direct intraorbital Coulomb repulsion for orbital α, $U_\alpha \equiv \langle \alpha, \alpha | \hat{\mathcal{V}}_c | \alpha, \alpha \rangle$, and $U_{\alpha\beta}$ is the direct interorbital Coulomb repulsion between electrons in two different orbitals, $U_{\alpha\beta} = \langle \alpha, \beta | \hat{\mathcal{V}}_c | \alpha, \beta \rangle$ for $\alpha \neq \beta$. $J_{\alpha\beta}$ is the Hund's rule coupling, i.e., the exchange integral of the Coulomb interaction, $J_{\alpha\beta} = \langle \alpha, \beta | \hat{\mathcal{V}}_c | \beta, \alpha \rangle$ for $\alpha \neq \beta$. Note that here we have split already the Hund's rule term into the density-density contribution (first term in the last line) and the spin-flip contrbition (last term). v_α are the orbital energies (single-particle energies) of the orbitals α which can be tuned by an external "gate" potential. From here on we will thus refer to v_α as the gate potential or simply gate for orbital α.

Here we work at (typically small) finite temperature T and consider the grand canonical ensemble (GCE). The corresponding density matrix (statistical operator) is thus given by

$$\hat{\Gamma} = \frac{e^{-\beta\mathcal{H}}}{Z} = \frac{1}{Z} \sum_m e^{-\beta E_m} |m\rangle\langle m| \qquad (2)$$

where $\beta = 1/T$ and Z is the GCE partition function with the chemical potential μ set to zero for convenience. The $|m\rangle$ are the many-body eigenstates of the QD and E_m the corresponding eigenenergies, i.e., $\mathcal{H}|m\rangle = E_m|m\rangle$. Note that in the absence of Hund's rule coupling ($J_{\alpha\beta} = 0$) the many-body eigenstates $|m\rangle$ are simply Slater determinants built from the single particle orbitals $|\phi_{\alpha\sigma}\rangle = c^\dagger_{\alpha\sigma}|0\rangle$ where $|0\rangle$ is the vacuum state.

The Hamiltonian Eq. (1) is very common in the fields of strongly correlated electrons and mesoscopic physics, as it provides a natural description of $3d$ or $4f$ shells of transition metal or lanthanide impurities in metallic hosts and of multiorbital QDs. In these systems, density-density interactions and Hund's rule coupling are by far the most important interactions. In particular, the role of the latter has become a focus of intense research in the field of strongly correlated electrons in recent years [46]. Alternatively, the Hamiltonian Eq. (1) may be viewed as a lattice Hamiltonian in the limit of vanishing hopping between sites which is similar to the point of view taken in strictly correlated DFT [47,48].

III. REVERSE-ENGINEERING OF HXC POTENTIALS AT FINITE TEMPERATURE

In our truncated Hilbert space, the density is uniquely defined by all occupancies $\boldsymbol{n} \equiv (n_1, \dots, n_\mathcal{M})$ of the QD orbitals. The Mermin theorem [49] (the finite-temperature version of the Hohenberg-Kohn theorem [1]) then establishes a one-to-one correspondence between the density (occupancies) $\boldsymbol{n}$ and the external potential (gate) $\boldsymbol{v} \equiv (v_1, \dots, v_\mathcal{M})$: $\boldsymbol{n} \overset{1-1}{\longleftrightarrow} \boldsymbol{v}$ or, in other words, the external potential is a functional of the occupancies, i.e., $v_\alpha = v_\alpha[\boldsymbol{n}]$.

In order to proceed we introduce the Kohn-Sham (KS) system, i.e., an effective noninteracting system that exactly reproduces the density $\boldsymbol{n}$ of the many-body Hamiltonian $\mathcal{H}$ [2]. Here the KS Hamiltonian is already diagonal in the original single-particle basis, i.e.,

$$\mathcal{H}^s = \sum_\alpha v^s_\alpha \, \hat{n}_\alpha. \qquad (3)$$

and the KS orbitals are identical to the original basis orbitals $|\phi^s_{\alpha\sigma}\rangle \equiv |\phi_{\alpha\sigma}\rangle$ with their eigenenergies given by the KS (gate) potentials v^s_α. The Hartree-exchange-correlation (Hxc) potentials v^{Hxc}_α are defined as the difference between the KS gate and the actual gate potential:

$$v^{\mathrm{Hxc}}_\alpha[\boldsymbol{n}] = v^s_\alpha[\boldsymbol{n}] - v_\alpha[\boldsymbol{n}]. \qquad (4)$$

The Hxc potential depends on the electron density which is completely determined by the occupancies $\boldsymbol{n}$ of the QD orbitals.

To determine the Hxc potential $\boldsymbol{v}^{\mathrm{Hxc}}$ as a functional of the density $\boldsymbol{n}$, the many-body problem given by $\mathcal{H}$ is solved for

a given set of gates $\boldsymbol{v}$. The resulting set of eigenstates and corresponding energies determines the density in the GCE according to:

$$n_\alpha = \mathrm{Tr}[\hat{\Gamma}\, \hat{n}_\alpha] = \frac{1}{Z} \sum_m \langle m|\hat{n}_\alpha|m\rangle e^{-\beta E_m}. \qquad (5)$$

The density in turn uniquely determines the KS potential and thus the Hxc potential. In our case of an isolated QD at finite temperature the occupancy n_α is simply determined by the gate v_α^s of a non-interacting QD, and is thus simply given by the Fermi-Dirac distribution, i.e. $n_\alpha = 2\, f(v_\alpha^s)$. Hence the KS gate for orbital α is given by $v_\alpha^s = \frac{1}{\beta}\ln\left(\frac{2}{n_\alpha}-1\right)$ and the corresponding Hxc potential can be obtained using Eq. (4) as

$$v_\alpha^{\mathrm{Hxc}} = \frac{1}{\beta}\ln\left(\frac{2}{n_\alpha}-1\right) - v_\alpha. \qquad (6)$$

Hence we have found the mapping $\boldsymbol{n} \longrightarrow \boldsymbol{v}^{\mathrm{Hxc}}$. By exploring the parameter space $\boldsymbol{v} = (v_1, \ldots, v_{\mathcal{M}})$, we can establish this mapping for the entire space of densities $\boldsymbol{n} = (n_1, \ldots, n_{\mathcal{M}})$ (for $n_\alpha \in [0, 2]$).

Hxc potentials and link to stability diagrams for the double quantum dot

We now focus on the two-orbital case, i.e., a DQD with generic density-density interactions (U_1, U_2, U_{12}). For the moment, we neglect Hund's rule coupling ($J_{12} = 0$), but we will discuss the effect of finite J_{12} later in Sec. IV C. The Hxc potentials can be constructed by reverse engineering as explained above. Here we are interested in the qualitative structure of the Hxc potentials, in particular in the positions (and heights) of step structures which appear in the low-temperature limit. In fact, these steps are not only the crucial but also the *only* features of the Hxc potential in the limit of low temperatures. In this section, we will show how these step structures can be deduced completely from the stability diagrams.

A stability diagram highlights the occupations (densities) of the ground states in the different regions of the plane of external gates v_1 and v_2. The position and shape of these regions in the v_1-v_2 plane depend on the values of the interaction parameters but within each region the pair of densities (n_1, n_2) remains constant at (close to) zero temperature and the possible values of the local densities n_i are restricted to 0, 1, and 2. For general temperatures, the domain of physically realizable densities is restricted to the square $0 \leqslant n_i \leqslant 2$. In this domain of densities, each of the nine pairs of densities (n_1, n_2) with $n_i \in \{0, 1, 2\}$ corresponds to a single point which we call a vertex. Therefore, a region of constant density in the stability diagram (i.e., in the v_1-v_2 plane) directly corresponds to a vertex (a single point) in the domain of realizable densities. A similar duality between regions in the plane of "potentials" and vertices in the plane of "densities" has also been observed in the framework of steady-state DFT (i-DFT) [50].

It turns out that the structure of the Hxc potentials (in the limit of low temperatures) for a given set of interaction parameters can be extracted just by looking at the stability diagram: For a given pair of ground state densities (or vertex in the density domain), one just needs to find all adjacent regions corresponding to a different vertex. Then the Hxc
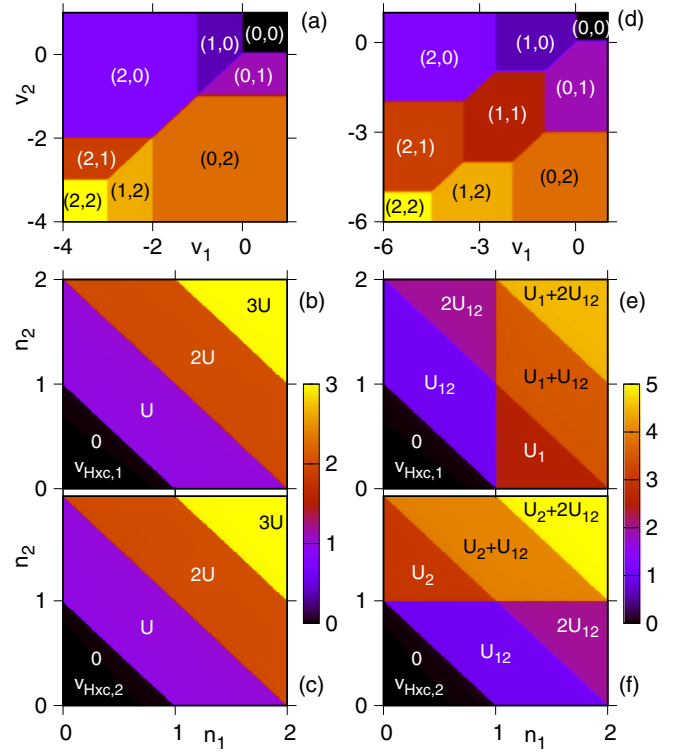

FIG. 1. Panels (a)–(c) (constant interaction model, CIM): Stability diagram (a) and Hxc potentials for orbitals 1 and 2 [panels (b) and (c), respectively] of the double quantum dot for $U_1 = U_2 = U_{12}$. Panels (d)–(f) (regime I): Stability diagram (d) and Hxc potentials for orbitals 1 and 2 [panels (e) and (f), respectively] of the double quantum dot for $U_1 = 2.5 U_{12}$, $U_2 = 3 U_{12}$. All energies in units of the smallest interaction (U_{12}).

potentials, which are functions of the density, will *only* contain steps which connect a given vertex (in the density domain) with those vertices corresponding to directly adjacent regions. The heights of these steps can also be extracted from the stability diagram. Below we will illustrate how this works, presenting some representative examples, and we will also explain the physical reasons behind our observations.

As a first example, we choose a simple one where all interaction parameters are equal, $U_1 = U_2 = U_{12}$. In this case, the total interaction can be written as $\frac{1}{2} U \hat{N}(\hat{N}-1)$, where $\hat{N} = \hat{n}_1 + \hat{n}_2$ is the operator for the total number of electrons on the dot. This model is known as the constant interaction model (CIM). It can be shown [51] that at zero temperature the Hxc potential v_α^{Hxc} of the CIM is independent of α and is a piecewise constant function of the total electron number N with discontinuous steps of height U whenever N crosses an integer. We mention that the CIM Hxc potential is strictly discontinuous only at zero temperature (this is a manifestation of the famous derivative discontinuity of DFT [10]). At finite but small temperature, the step structure persists but the Hxc potentials are now continuous functions of the densities [52].

We now show how the known CIM Hxc potentials (at low temperature) can be inferred directly from the stability diagram. This diagram is shown in Fig. 1(a) for the CIM with $U_1 = U_2 = U_{12} = 1$. Here the regions corresponding to the different possible ground-state densities (given in parenthesis)

are marked by different colors. The reverse-engineered Hxc potentials for orbitals 1 and 2 are shown in Figs. 1(b) and 1(c), respectively. In the stability diagram, the domain corresponding to the occupation (0,0) is directly adjacent only to the domains with occupations (1,0) and (0,1). If we connect the (0,0) vertex with one of those vertices in the n_1-n_2 plane, we see that the resulting lines run along the border of the allowed density domain. The complete set of lines along the borders of the density domain follow from the sequence of vertices $(0, 0) \rightarrow (1, 0) \rightarrow (2, 0)$, $(0, 0) \rightarrow (0, 1) \rightarrow (0, 2)$, $(2, 0) \rightarrow (2, 1) \rightarrow (2, 2)$, and $(0, 2) \rightarrow (1, 2) \rightarrow (2, 2)$. The only other possibilities of connecting vertices corresponding to adjacent regions in the $v_1 - v_2$ plane are (i) $(1, 0) \rightarrow (0, 1)$, (ii) $(2, 0) \rightarrow (0, 2)$, and (iii) $(2, 1) \rightarrow (1, 2)$. These lines are exactly the position of the steps at integer $N = n_1 + n_2$ in the Hxc potentials, see Figs. 1(b) and 1(c). Moreover, the height of these steps can also be deduced from the stability diagram: consider a $v_2 > 0$ such that the second dot is always empty, independent of v_1. Then we have essentially a single-site model (SSM) in contact with a particle and heat bath because the second dot doesn't contribute. However, we know that the the Hxc potential of a SSM in the low-temperature limit is a step function with step of height U at half filling [43]. In a self-consistent DFT calculation, this step in the Hxc potential leads to a pinning of the KS level to the Fermi energy over a range of gates of width U. Therefore, the width (in v_1) of the (1,0) region is just $U_1 = U$. Similarly, the width (in v_2) of the (0,1) region is $U_2 = U$. The line in the stability diagram where the (1,0) and (0,1) regions touch is the line $v_1 = v_2$ for which the states with the corresponding occupations are degenerate. The KS system is a system of effectively noninteracting electrons which reproduces the interacting density. However, for a noninteracting double dot with potentials v_1^s and v_2^s the *only* possibility for the half-filled dots to be degenerate is for the point $v_1^s = v_2^s = \ln 3/\beta$ which in the limit of zero temperature approaches $v_1^s = v_2^s = 0$. Therefore, to reproduce the degeneracy as observed in the stability diagram, the KS potential for *both* orbitals has to be pinned over an interval of range U. This can only be achieved if the Hxc potentials for both orbitals have steps at $N = 1$ of height U as observed in the reverse-engineered Hxc potentials. On the line $v_1 = v_2$ also the states with occupations (2,0) and (0,2) as well as the ones with occupations (2,1) and (1,2) are degenerate. It is easy to show that along this line the states with occupations (2,0) and (0,2) are lowest in energy for the region $-U > v_1 > -2U$. For noninteracting systems, again there is only one point ($v_1^s = v_2^s = 0$) for which the states with (2,0) and (0,2) are degenerate. Therefore, the Hxc potentials have to be such that for the range of gates $-U > v_1 > -2U$, the KS potentials are pinned to zero. This can only be achieved if both Hxc potentials exhibit a step of height U at $N = 2$, as observed. Finally, there is yet another step of height U in both Hxc potentials for $N = 3$ which follows in a similar way from the analysis of the contact line between the (2,1) and (1,2) regions. In this way, we have therefore been able to reconstruct the Hxc potentials of the CIM only by analyzing the stability diagram.

In the second example, we make all the interaction parameters different from each other, i.e., the levels are now not equivalent anymore. Moreover, we choose the interdot

interaction U_{12} to be smaller than both U_1 and U_2. This parameter regime ($U_{12} < U_1, U_2$) we denote as regime I, see discussion in Sec. IV A. In the stability diagram for this regime [Fig. 1(d)] we now have a new region with densities (1,1) showing up. To deduce the low-temperature Hxc potentials (reverse-engineered results shown in Figs. 1(e) and 1(f)), we begin by looking at the regions with occupations (1,0) and (0,1). The corresponding states are degenerate along the line $v_1 = v_2$ and for $-U_{12} < v_1 < 0$ they are the ground states of the double dot. For the KS system to reproduce this density for external potentials $v_1 = v_2$ in the same interval, we need the KS potentials on both orbitals to be pinned to the Fermi energy. Therefore, both Hxc potentials need to exhibit a step of height U_{12} along the line connecting the vertices (1,0) and (0,1). If one of the levels is completely empty, the other level essentially behaves like a SSM (see discussion of the previous example). Therefore, for the Hxc potential of orbital 1 we have $v_1^{\text{Hxc}}(n_1, 0) = U_1$ for $1 < n_1 < 2$ while $v_2^{\text{Hxc}}(0, n_2) = U_2$ for $1 < n_2 < 2$. The regions (1,0) and (1,1) are adjacent along the line $v_1 = -U_{12}$ for $-U_1 < v_1 < -U_{12}$ and thus the KS potential of the first orbital needs to be pinned to the Fermi energy for this range of v_1, leading to a step of height $U_1 - U_{12}$ along the line connecting the (1,0) and (1,1) vertices for v_1^{Hxc}. Similarly, v_2^{Hxc} needs to exhibit a step of height $U_2 - U_{12}$ along the line connecting the (0,1) and (1,1) vertices. Next, the regions (2,0) and (1,1) are adjacent for $-U_{12} - U_\alpha < v_\alpha < -U_\alpha$ ($\alpha = 1, 2$) and therefore both Hxc potentials have a step of height U_{12} along the lines connecting the (2,0) and (1,1) vertices. Similarly, there also has to be a step of height U_{12} in both Hxc potentials along the line connecting the (0,2) and (1,1) vertices. The regions (1,1) and (1,2) are adjacent for $-2U_{12} < v_1 < -U_1 - U_{12}$, leading to a step of height $U_1 - U_{12}$ in v_1^{Hxc} along the line $(1, 1) \rightarrow (1, 2)$. Similarly, there is a step of height $U_1 - U_{12}$ in v_2^{Hxc} along the $(1, 1) \rightarrow (2, 1)$ line. Finally, the regions (2,1) and (1,2) are adjacent along a line of length U_{12}, leading to a step of this height in both Hxc potentials along the $(2, 1) \rightarrow (1, 2)$ line. In this way, we now have completely determined the (low temperature) Hxc potentials of both orbitals just by analyzing the stability diagram. Their overall structure is such that they exhibit steps for integer total occupation $N = n_1 + n_2$ for both Hxc potentials plus an additional step at $n_\alpha = 1$ for v_α^{Hxc}. Note also that for the special case $U_{12} = 0$, only the steps at $n_\alpha = 1$ for v_α^{Hxc} survive while those at integer N disappear. This is not surprising since in this case our model just describes two completely independent single impurities and, naturally, the corresponding Hxc potential for orbital α is completely independent of the other orbital and given by the Hxc potential of a SSM with interaction strength U_α. This has also been discussed as "intrasystem steps" in Ref. [53].

We have identified two further parameter regimes for the interaction parameters (see Sec. IV A) where qualitative changes both in the stability diagram as well as in the Hxc potentials occur. In both regimes, the interorbital interaction U_{12} is smaller than at least one of the intraorbital ones. Without loss of generality, we may assume $U_1 \leqslant U_2$. In regime II we have $U_1 < U_{12} < (U_1 + U_2)/2$ while regime III is defined by $U_1 \leqslant (U_1 + U_2)/2 \leqslant U_{12}$. In Figs. 2(a)–2(c), we show the stability diagram and Hxc potentials for interaction parameters chosen in regime II. Compared to regime I [Figs. 1(d)–1(f)],
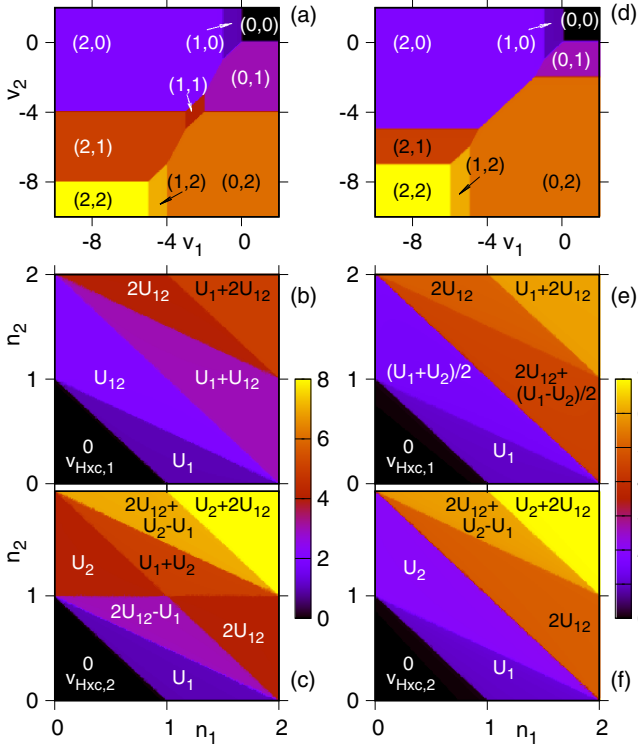
FIG. 2. Panels (a)–(c) (regime II): Stability diagram (a) and Hxc potentials for orbitals 1 and 2 [panels (b) and (c), respectively] of the double quantum dot for $U_2 = 4U_1$ and $U_{12} = 2U_1$. Panels (d)–(f) (regime III): stability diagram (d) and Hxc potentials for orbitals 1 and 2 [panels (e) and (f), respectively] of the double quantum dot for $U_2 = 2U_1$, and $U_{12} = 2.5U_1$. All energies in units of the smallest interaction (U_1).

in the stability diagram we now find that there exists a range of potentials for which regions (2,0) and (0,1) are directly adjacent and similarly for regions (2,1) and (0,2). As expected, these transitions lead to the new steps in the Hxc potentials. On the other hand, for the Hxc potential of orbital 1 the step at $n_1 = 1$ (present in regime I) now disappears while in $v_{\text{Hxc},2}$ the step at $n_2 = 1$ survives (this step is related to the vertical lines delimiting the (1,1) region in the stability diagram). We have annotated the plateau values in both Hxc potentials, which can be found by analyzing the stability diagram using similar arguments to the ones used above for regime I.

Finally, in Figs. 2(d)–2(f), we show the stability diagram and Hxc potentials for interaction parameters chosen in regime III. Compared to regime II, the main qualitative difference is the disappearance of the step at $n_2 = 1$ in the Hxc potential of orbital 2. Again, all the step structures in the Hxc potentials can fully be deduced by analyzing the stability diagram.

Before we close this section, we would like to mention that for multilevel dots beyond the double dot studied here, in principle the analysis of the (multidimensional) stability diagram(s) also allows for a complete deduction of the low-temperature Hxc potentials of the different orbitals. However, it is clear that this procedure rapidly becomes quite cumbersome as the number of levels increases.

IV. MODELLING OF THE HXC POTENTIALS

A. Decomposition of the interaction into basic building blocks

In the following, we show that the Hxc potentials for generic density-density interactions can be built from a few basic potentials. We start with the most common (or natural) situation where the interorbital interaction U_{12} is smaller than both of the intraorbital ones, $U_{12} \leqslant U_1, U_2$. A specific case with $U_{12} < U_1 < U_2$ was studied in the previous section [see Figs. 1(d)–1(f)]. The corresponding Hxc potential shows steps at integer values of $N = n_1 + n_2$, connected to a CIM potential, as well as steps at $n_1 = 1$ for orbital 1 or at $n_2 = 1$ for orbital 2 connected to a SSM potential of the corresponding orbital.

This suggests that in the regime $U_{12} \leqslant U_1, U_2$ the Hxc potential for each orbital may be built from a superposition of a CIM potential plus a SSM potential. We can rationalize this idea by a decomposition of the Coulomb interaction term as follows. Rewriting the interorbital repulsion as

$$U_{12}\, \hat{n}_1\, \hat{n}_2 = \frac{U_{12}}{2}\hat{N}(\hat{N}-1) - U_{12}\sum_\alpha \hat{n}_{\alpha\uparrow}\hat{n}_{\alpha\downarrow}, \quad (7)$$

we can split the interaction into a CIM part and two SSM interactions (one for each orbital):

$$\mathcal{V}_{\text{int}} = \frac{1}{2}U_{12}\hat{N}(\hat{N}-1) + \sum_\alpha \delta U_\alpha\, \hat{n}_{\alpha\uparrow}\hat{n}_{\alpha\downarrow}, \quad (8)$$

where $\delta U_\alpha \equiv U_\alpha - U_{12}$ is the "excess interaction" for each orbital. This suggests we write the Hxc potential for level α for regime I ($U_{12} \leqslant U_1, U_2$) as the sum of the CIM Hxc potential for interaction U_{12} and the SSM potential for δU_α,

$$v_\alpha^{\text{Hxc}}[\boldsymbol{n}] = v_{\text{CIM}}^{\text{Hxc}}(U_{12})[N] + v_{\text{SSM}}^{\text{Hxc}}(\delta U_\alpha)[n_\alpha], \quad (9)$$

where $N = n_1 + n_2$.

Now if U_{12} is larger than at least one of the intraorbital interactions U_α, this decomposition of the Coulomb interaction obviously leads to negative interactions δU_α in the SSM parts. Since the step in the Hxc potential of the SSM at $n_\alpha = 1$ would actually vanish for negative interactions [54], in this regime the step structure can obviously not be rationalized by the above decomposition of the interaction. Indeed the structure of the reverse-engineered Hxc potentials (Fig. 2) appears to be quite different from that for the regime $U_{12} \leqslant U_\alpha$. Essentially, two new features are found in this regime: (i) an increase of the step height at $N = 2$ with respect to the CIM potential, and (ii) peculiar new steps at integer values of $n_1/2 + n_2$. The steps at integer $n_1/2 + n_2$ are generated by a peculiar interaction of the form

$$\mathcal{V}_{\text{skew}} = \frac{U}{2}\hat{n}_2(\hat{N}-1), \quad (10)$$

which we will refer to as *skew interaction* from now on. This interaction is realized by setting $U_1 = 0$ and $U_{12} = U_2/2 = U/2$. The corresponding stability diagram and the Hxc potential for orbital 2 are shown in Figs. 3(a) and 3(b), respectively. Note that the Hxc potential of orbital 1 has the same structure but the step heights are lower by a factor of 1/2.

Common to all cases is that there is always a contribution of the CIM potential, as long as all interactions (U_1, U_2, U_{12})
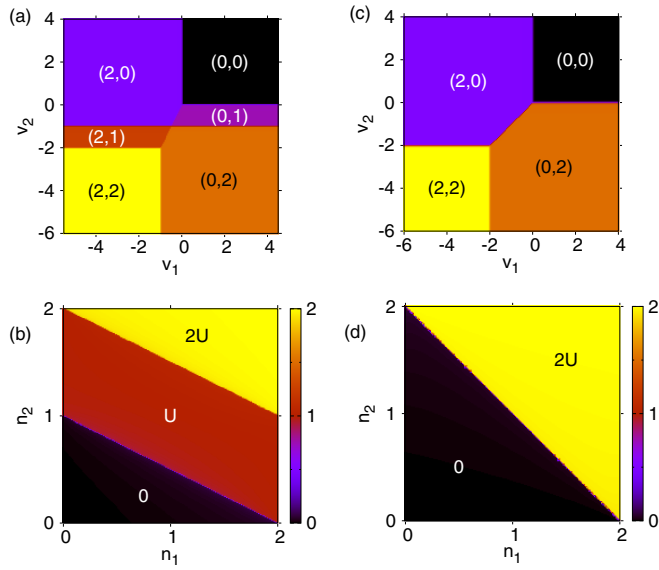
FIG. 3. Panels (a), (b) stability diagram (a) and Hxc potential of orbital 2 (b) for the skew interaction $\mathcal{V}_{\text{skew}} = \frac{U}{2}\hat{n}_2(\hat{N}-1)$. The structure of the Hxc potential for orbital 1 is the same as for orbital 2 but the step heights are half those of orbital 2 $(0, U/2, U)$. Panels (c), (d) stability diagram (c) and Hxc potential of both orbitals (d) for the interorbital interaction $\mathcal{V}_{\text{inter}} = U\hat{n}_1\hat{n}_2$. All energies in units of U in both cases.

remain finite. This contribution is given by the smallest interaction. In the case that U_{12} is larger than at least one of the intraorbital interactions U_α, we may assume without loss of generality that U_1 is the smallest interaction. Subtracting the CIM interaction $\sim U_1$ from the total interaction thus yields

$$\mathcal{V}_{\text{int}} - \frac{U_1}{2}\hat{N}(\hat{N}-1)$$
$$= (U_{12} - U_1)\, n_1 n_2 + (U_2 - U_1)\, n_{2\uparrow} n_{2\downarrow}$$
$$= (U_{12} - U_1)\, n_1 n_2 + \frac{U_2 - U_1}{2}\, n_2(n_2 - 1), \quad (11)$$

where in the last term we have rewritten the intraorbital interaction for orbital 2 in terms of $n_2 = n_{2\uparrow} + n_{2\downarrow}$ instead of $n_{2\uparrow}$ and $n_{2\downarrow}$. Hence the remaining interaction consists of an interorbital interaction $\sim(U_{12} - U_1)$ and a SSM interaction $\sim(U_2 - U_1)/2$ for orbital 2. These two terms can be combined to yield the skew interaction and a remaining term. Depending on whether $U_{12} - U_1$ is larger or smaller than $(U_2 - U_1)/2$, the remaining term is either a SSM interaction for orbital 2 if $U_{12} - U_1 < (U_2 - U_1)/2$ [or, equivalently $U_{12} < U_{\text{ave}} \equiv (U_1 + U_2)/2$] or an interorbital interaction if $U_{12} - U_1 > (U_2 - U_1)/2$ (or equivalently $U_{12} > U_{\text{ave}}$).

We thus identify two new regimes in addition to regime I ($U_{12} \leqslant U_\alpha$) discussed above: In regime II, the interorbital interaction U_{12} takes values between the lowest interaction of both intraorbital interactions and their average U_{ave}, i.e., $U_1 < U_{12} < U_{\text{ave}}$. This is the case shown in Figs. 2(a)–2(c). After subtraction of the CIM potential $\sim U_1$, we find that the remaining interaction in regime II can be written as

$$(U_{12} - U_1)\hat{n}_2\,(\hat{N}-1) + 2(U_{\text{ave}} - U_{12})\hat{n}_{2\uparrow}\hat{n}_{2\downarrow}. \quad (12)$$

Overall, this suggests the following decomposition of the Hxc potential in regime II ($U_1 < U_{12} < U_{\text{ave}}$):

$$v_\alpha^{\text{Hxc}}[\boldsymbol{n}] = v_{\text{CIM}}^{\text{Hxc}}(U_1)[N] + v_{\text{skew},\alpha}^{\text{Hxc}}(2(U_{12} - U_1))[\boldsymbol{n}]$$
$$+ v_{\text{SSM}}^{\text{Hxc}}(2(U_{\text{ave}} - U_{12}))[n_2]\,\delta_{\alpha 2}, \quad (13)$$

where $\delta_{\alpha 2}$ is the Kronecker delta which ensures that the SSM term only contributes to the Hxc potential of orbital 2. Note that as $U_{12} \to U_{\text{ave}}$ the SSM term vanishes.

On the other hand, regime III occurs when the interorbital interaction exceeds the average intraorbital interaction, i.e., $U_{12} > U_{\text{ave}} > U_1$. This was the case considered in Figs. 2(d)–2(f). In this regime, the remaining interaction after subtraction of the CIM $\sim U_1$ can be rewritten in terms of the skew interaction Eq. (10) and a pure interorbital interaction part:

$$\frac{U_2 - U_1}{2}\,\hat{n}_2\,(\hat{N}-1) + (U_{12} - U_{\text{ave}})\,\hat{n}_1\hat{n}_2. \quad (14)$$

As can be seen in Fig. 3(d), this interorbital term,

$$\mathcal{V}_{\text{inter}} = U\hat{n}_1\hat{n}_2, \quad (15)$$

gives rise to a single step at $N = 2$ which explains the increase in step height at $N = 2$ with respect to the CIM, observed in Figs. 2(e) and 2(f). Overall, this suggests the following decomposition of the Hxc potential in regime III ($U_{12} > U_{\text{ave}} > U_1$):

$$v_\alpha^{\text{Hxc}}[\boldsymbol{n}] = v_{\text{CIM}}^{\text{Hxc}}(U_1)[N] + v_{\text{skew},\alpha}^{\text{Hxc}}(U_2 - U_1)[\boldsymbol{n}]$$
$$+ v_{\text{inter}}^{\text{Hxc}}(U_{12} - U_{\text{ave}})[n_1 + n_2]. \quad (16)$$

We can see that for $U_1 = U_2$ the skew part of the Hxc potential disappears.

Hence we have found a decomposition of the Hxc potential for a two-orbital model with generic (density-density) interactions in all three regimes in terms of four basic potentials which are shown schematically in Fig. 4. We would like to emphasize at this point that regime I corresponds to a more natural choice of parameters than the other two regimes, since the interorbital interaction U_{12} is generally smaller than any of the intra-orbital interactions U_α. Nevertheless, the other regimes might be realized by effective models or possibly by screening of the Coulomb interactions. In the next section we will present parametrizations of the Hxc potentials in the different regimes, making use of its decomposition into the basic building blocks shown in Fig. 4.

B. Generalization of Hxc potential to more than two orbitals

For specific choices of parameters we can generalize the Hxc potential for the DQD to an arbitrary number of orbitals in a straightforward manner. We concentrate on the physically most relevant regime I ($U_\alpha, U_\beta > U_{\alpha\beta}$). If we choose the inter-orbital interaction to be constant, $U_{\alpha\beta} \equiv U'$, which thus has to be smaller than *all* of the intraorbital interactions, $U' < U_\alpha$, we can rewrite the interaction in a similar manner as in Eq. (8) in terms of a CIM term $\sim U'$ for all the electrons $N = \sum_\alpha n_\alpha$ and SSM terms $\sim \delta U_\alpha \equiv U_\alpha - U'$ for the individual orbitals as

$$\mathcal{V}_{\text{int}} = \frac{1}{2}U'\hat{N}(\hat{N}-1) + \sum_\alpha \delta U_\alpha\, \hat{n}_{\alpha\uparrow}\hat{n}_{\alpha\downarrow}, \quad (17)$$
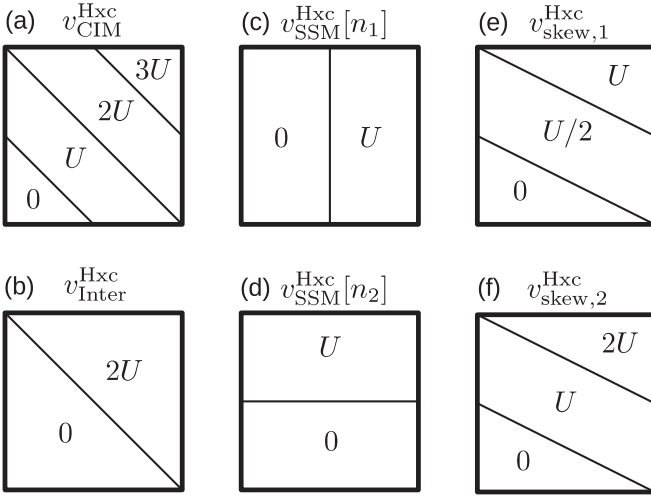
FIG. 4. Schematic representation of the four basic Hxc potentials for building the generic potentials for all three regimes. (a) Hxc potential for CIM interaction $\frac{U}{2}\hat{N}(\hat{N}-1)$. (b) Hxc potential for inter-orbital interaction $U n_1 n_2$. (c), (d) Hxc potential for intraorbital (i.e., SSM) interactions $U n_{\alpha\uparrow} n_{\alpha\downarrow}$. (e), (f) Hxc for the skew interaction $\frac{U}{2}\hat{n}_2(\hat{N}-1)$.

where $\delta U_\alpha = U_\alpha - U'$. This suggests we decompose the XC functionals in complete analogy to the two-orbital case in regime I as

$$v_\alpha^{\text{Hxc}}[\boldsymbol{n}] = v_{\text{CIM}}^{\text{Hxc}}(U')[N] + v_{\text{SSM}}^{\text{Hxc}}(\delta U_\alpha)[n_\alpha]. \quad (18)$$

In Sec. V B, we will see that this decomposition of the Hxc potential leads to excellent results for multiorbital QDs. For a more general choice of interaction parameters, the above decomposition is likely to become more complicated. This will be the focus of future work.

C. The effect of Hund's rule coupling

So far, we have neglected the effect of Hund's rule coupling on the Hxc potentials. In Fig. 5, we show the stability diagram and the corresponding reverse-engineered Hxc potential for the case of a CIM-type direct interaction part ($U_1 = U_2 = U_{12} \equiv U$) plus the full Hund's coupling contri-
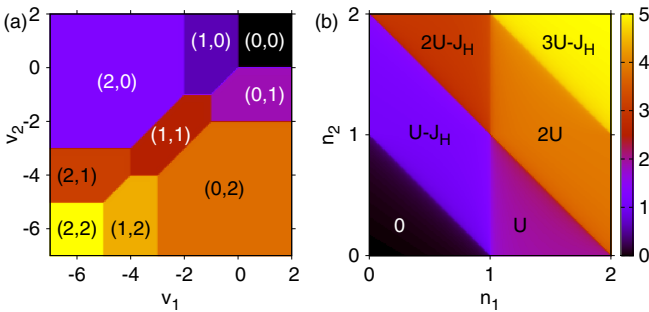

FIG. 5. Effect of Hund's rule coupling on (a) stability diagram and (b) Hxc potential of orbital 1 for CIM interaction plus Hund's rule coupling, $\mathcal{V}_{\text{int}} = \frac{U}{2}\hat{N}(\hat{N}-1) + \mathcal{V}_{\text{Hund}}$ for $U = 2J_H$. Here, due to symmetry, the Hxc potential for orbital 2 can simply be obtained by reflection along the $n_1 = n_2$ line. All energies in units of J_H.

bution ($J_H \equiv J_{12}$). Both the stability diagram and the reverse-engineered Hxc potential shown in Fig. 5 resemble the ones for the case with $U_{12} < U_\alpha$ without Hund's coupling [cf. Figs. 1(d)–1(f)]. Only the size of the vertex regions changes in the stability diagram, and correspondingly in the Hxc potentials only the step heights change. Moreover, by switching off the spin-flip term in Eq. (1), we find that it does not have any effect on the densities and, consequently, on the Hxc potentials and thus can be neglected. Hence, in the following considerations we only need to take into account the density-density part of the Hund's coupling [next to last term in Eq. (1)].

In the spirit of the previous section, we can rewrite the density-density part of the Hund's rule coupling term in terms of a (negative) CIM interaction and (positive) SSM interactions for the remaining orbitals plus a remaining *positive* interaction part:

$$\mathcal{V}_H = -J_H \sum_\sigma \hat{n}_{1\sigma}\hat{n}_{2\sigma} = -J_H \hat{n}_1 \hat{n}_2 + J_H \sum_\sigma \hat{n}_{1\sigma}\hat{n}_{2\bar{\sigma}}$$

$$= -\frac{J_H}{2}\hat{N}(\hat{N}-1) + J_H \sum_\alpha \hat{n}_{\alpha\uparrow}\hat{n}_{\alpha\downarrow} + J_H \sum_\sigma \hat{n}_{1\sigma}\hat{n}_{2\bar{\sigma}}, \quad (19)$$

where in the last term $\bar{\sigma}$ denotes the opposite spin of σ. The last term gives rise to a step at $N = 2$ in the Hxc potential similar to the interorbital interaction term but with step height J_H instead of $2U$ [cf. Fig. 3(d)].

When adding the density-density contribution of the Hund's rule coupling to the direct interaction part in regime I ($U_{12} \lesssim U_1, U_2$), we can rewrite the interaction in terms of a CIM interaction, SSM terms, and the last term of the Hund's density-density interaction Eq. (19) as

$$\mathcal{V}_{\text{int}} = \frac{U_{12} - J_H}{2}\hat{N}(\hat{N}-1) + \sum_\alpha (\delta U_\alpha + J_H)\hat{n}_{\alpha\uparrow}\hat{n}_{\alpha\downarrow}$$

$$+ J_H \sum_\sigma \hat{n}_{1\sigma}\hat{n}_{2\bar{\sigma}}, \quad (20)$$

where, as defined in the previous section, $\delta U_\alpha = U_\alpha - U_{12}$. Hence all terms can be modeled by the basic Hxc potentials shown in Fig. 4:

$$v_\alpha^{\text{Hxc}}[\boldsymbol{n}] = v_{\text{CIM}}^{\text{Hxc}}(U_{12} - J_H)[N] + v_{\text{SSM}}^{\text{Hxc}}(\delta U_\alpha + J_H)[\boldsymbol{n}]$$

$$+ v_{\text{inter}}^{\text{Hxc}}(J_H/2)[n_1 + n_2]. \quad (21)$$

D. Parametrization of the basic Hxc potentials

In the zero-temperature limit, the steps in the Hxc potential become infinitely sharp and thus can be described by simple step functions. At finite temperature, however, the steps are broadened in a nontrivial way. For the SSM at finite temperature, an *exact* expression for the Hxc potential can be derived [52],

$$v_{\text{SSM}}^{\text{Hxc}}[n] = U + \frac{1}{\beta}\ln\left(\frac{x + \sqrt{x^2 + e^{-\beta U}(1 - x^2)}}{1 + x}\right), \quad (22)$$

where $x = n - 1$.

In the following, we will use the Hxc functional for the SSM as the basis for constructing approximations for the other
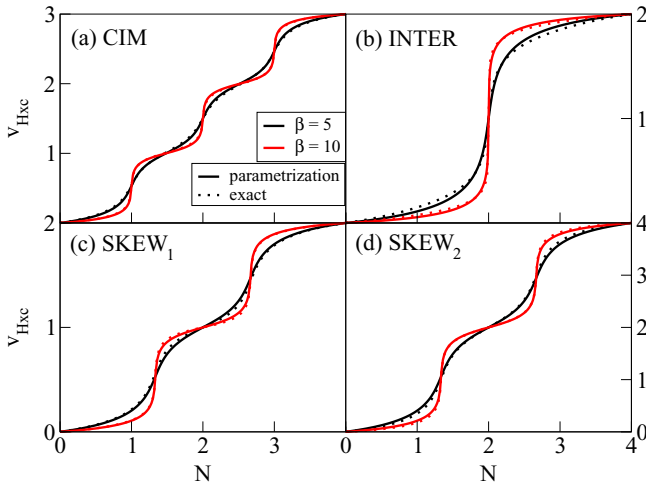
FIG. 6. Comparison of parametrized and exact Hxc potentials as a function of $N = n_1 + n_2$ for three basic interactions: (a) CIM interaction ($U_1 = U_2 = U_{12} > 0$); (b) interorbital interaction ($U_{12} > 0$ and $U_1 = U_2 = 0$); (c) and (d) skew interaction ($U_2 = 2U_{12} > 0$ and $U_1 = 0$); all energies in units of the smallest nonzero interaction (U_{12}).

three basic Hxc potentials into which the generic Hxc potential can be decomposed, namely, the CIM, the interorbital, and the skew potential (see Fig. 4). We start with the CIM potential and show that an excellent parametrization of the Hxc potential can be achieved by simply summing the (exact) SSM potential Eq. (22) over the charging states of the dot, and shifting and rescaling it such that the potential does not become negative or larger than $(2\mathcal{M} - 1)U$:

$$v_{\text{CIM}}^{\text{Hxc}}[N] = \frac{(2\mathcal{M} - 1)U}{v_{\text{CIM}}^{\max}} \sum_{J=1}^{2M-1} \left[v_{\text{SSM}}^{\text{Hxc}}[N - J + 1] \right.$$
$$\left. - v_{\text{SSM}}^{\text{Hxc}}[-J + 1] \right], \quad (23)$$

where

$$v_{\text{CIM}}^{\max} = \sum_{J=1}^{2M-1} \left[v_{\text{SSM}}^{\text{Hxc}}[2\mathcal{M} - J + 1] - v_{\text{SSM}}^{\text{Hxc}}[-J + 1] \right] \quad (24)$$

is the maximal value that the sum in Eq. (23) aquires at $N = 2\mathcal{M}$. The prefactor $(2\mathcal{M} - 1)U/v_{\text{CIM}}^{\max}$ thus rescales the potential such that the potential yields the exact value $(2M - 1)U$ at $N = 2\mathcal{M}$. As can be seen in Fig. 6(a), the agreement with the exact result is quite remarkable.

For the interorbital potential, we find a good parametrization describing the step at total $N = 2$ again in terms of the SSM potential, as

$$v_{\text{inter}}^{\text{Hxc}}(U, \beta)[N] = v_{\text{SSM}}^{\text{Hxc}}(2U, \beta^*)[N/2], \quad (25)$$

where we have replaced the actual inverse temperature β by an effective reduced value, $\beta^* = 0.73\beta$ and the step height is increased by a factor of 2 compared to the SSM. The agreement with the exact potential is very good, as can be seen in Fig. 6(b).

Finally, for the skew interaction, we parametrize the Hxc potential in a similar way as the Hxc potential for the CIM, by summing two SSM potentials, one for each of the steps,

and shifting and rescaling so the potential does not become negative or larger than the maximum value:

$$v_{\text{skew},\alpha}^{\text{Hxc}}(U)[\boldsymbol{n}] = \frac{\alpha U}{v_{\text{skew}}^{\max}} \sum_{J=0,1} \left\{ v_{\text{SSM}}^{\text{Hxc}}\left(\frac{U}{2}\right)\left[\frac{n_1}{2} + n_2 - J\right] \right.$$
$$\left. - v_{\text{SSM}}^{\text{Hxc}}\left(\frac{U}{2}\right)[-J] \right\}, \quad (26)$$

where

$$v_{\text{skew}}^{\max} = \sum_{J=0,1} \left\{ v_{\text{SSM}}^{\text{Hxc}}\left(\frac{U}{2}\right)[3 - J] - v_{\text{SSM}}^{\text{Hxc}}\left(\frac{U}{2}\right)[-J] \right\}. \quad (27)$$

Also here the agreement with the exact potential is very good as can be seen in Figs. 6(c) and 6(d).

We have thus found parametrizations of the four basic Hxc potentials. It should be noted, however, that at higher temperatures the exact CIM and interorbital potentials (which in the zero temperature limit only depend on total N) also acquire a dependence on the difference $\delta N \equiv n_1 - n_2$ which has not been taken into account here. This discrepancy of our parametrizations might be responsible for some of the moderate deviations of our DFT results from the exact ones discussed in the next section.

V. DFT CALCULATIONS

We are now going to apply the above-developed parametrization of the Hxc potential in actual DFT calculations. To this end, we solve the KS equations which for the multiorbital QD in the GCE are given by

$$n_\alpha = 2 f(v_\alpha + v_{\text{Hxc}}[\boldsymbol{n}]) \quad \text{for } \alpha = 1 \ldots \mathcal{M}. \quad (28)$$

Since the sharp step features in the Hxc potentials are expected to prevent the convergence of the usual self-consistency procedure in the density [55], here we make use instead of a multidimensional generalization of the bisection approach as proposed before in Ref. [55] for finding the root of the multidimensional function:

$$F_\alpha[\boldsymbol{n}] \equiv n_\alpha - 2 f(v_\alpha + v_{\text{Hxc}}[\boldsymbol{n}]). \quad (29)$$

In the following, we study the evolution of the density $\boldsymbol{n}$ of multiorbital QDs as a function of the applied gate v_g for different parameter sets. The gate v_g exerts a total shift of the QD levels ϵ_α and hence the total gate for orbital α is given by

$$v_\alpha = \epsilon_\alpha + v_g. \quad (30)$$

Consequently, the differences in the gate potentials between different orbitals remain constant as the gate v_g changes, $\delta v_{\alpha\beta} \equiv v_\alpha - v_\beta = \epsilon_\alpha - \epsilon_\beta$. In the following, we will usually take the particle-hole symmetric (phs) point given by $\epsilon_\alpha^* = -\frac{U_\alpha}{2} - \sum_{\beta \neq \alpha} U_{\alpha\beta}$ as the reference system.

A. Results for the double quantum dot

We now study the DQD, and start by considering the degenerate case in regime I, i.e., $U_1 = U_2 > U_{12}$, where $\delta N = 0$. Figure 7 compares the exact densities with the ones computed in DFT using the Hxc potential for regime I, Eq. (9), together with the parametrizations of the SSM, Eq. (22), and the CIM, Eq. (23), respectively. We see that the DFT
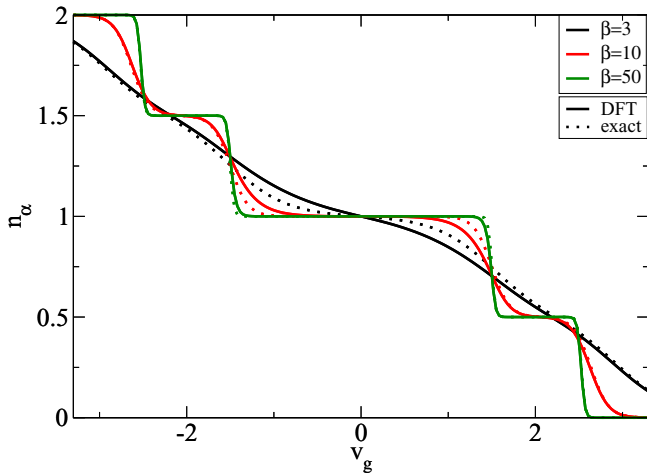
FIG. 7. Density $\boldsymbol{n} = (n_1, n_2)$ as function of the gate voltage v_g for different temperatures when $U_1 = U_2 = 3U_{12} > 0$ (regime I). The DFT result (solid line) is practically on top of the GCE result (dashed line) in the low temperature regime. All energies in units of the smallest interaction U_{12}.

FIG. 9. (a) Comparsion of the evolution of the density $\boldsymbol{n} = (n_1, n_2)$ with the gate voltage v_g in regime II ($U_2 = 2U_{12} = 4U_1$) and regime III ($U_2 = U_{12} = 4U_1$). (b) Comparison of density evolution for two different values of the splitting δv in regime II ($U_{12} = 2U_1$). The inset shows the different paths in the density plane. $\beta = 20/U_1$ everywhere. All energies in units of U_1.

results correctly describe all the features of the densities as a function of the gate. At low temperatures, the width of the central step (around $v_g = 0$) is given by U_i while the other two step widths correspond to U_{12}. At higher temperatures, our parametrization leads to moderate discrepancies in the slopes of the central step that disappear as the temperature approaches zero.

Next we consider the situation where the intraorbital Coulomb repulsions are different, $U_1 > U_2 > U_{12}$. In Figs. 8(a) and 8(b), the occupations n_i are presented as a function of the gate v_g for two different temperatures. At low temperatures [Fig. 8(a)] at large negative gate voltage ($v_g < -2.5$), both orbitals of the DQD are completely filled
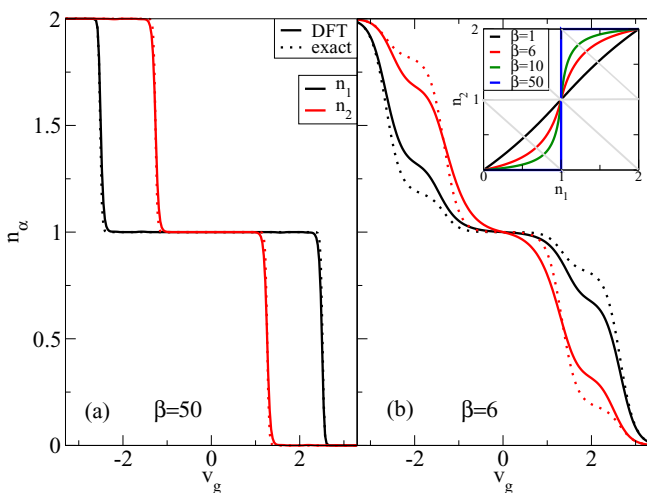

FIG. 8. Density $\boldsymbol{n} = (n_1, n_2)$ as a function of the gate voltage v_g for $U_1 = 3U_{12}$, $U_2 = 2.5U_{12}$ (regime I) for (a) low and (b) high temperatures. The inset of panel (b) shows the path in the $n_1 - n_2$ plane as the gate is varied for different temperatures. The grey lines show the steps of the CIM and SSM terms that appear in the Hxc potentials. All energies in units of the smallest interaction U_{12}.
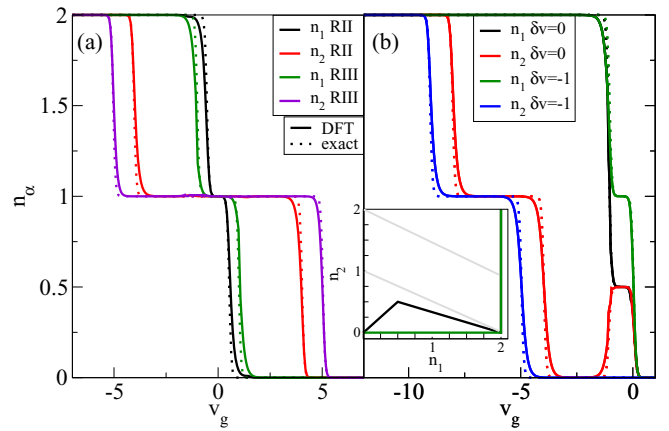
($n_\alpha \sim 2$). As the gate is increased, first the orbital with the higher interaction (U_1) becomes half filled around $v_g \sim -2.5$, and then around $v_g \sim -1.5$ also the orbital with the lower interaction (U_2) becomes half filled. Upon further increase of the gate, the sequence of emptying is reversed, as first the orbital with the higher interaction and thus lower gate (v_2) is emptied around $v_g \sim 1.5$ and finally the orbital with lower interaction and thus higher gate (v_1) is emptied. At higher temperatures, extra steps develop in the evolution of the density versus gate voltage, as can be seen in Fig. 8(b). The appearance of new steps can be understood by the path taken in the $n_1 - n_2$ plane as the gate voltage changes, shown in the inset of Fig. 8(b) for different temperatures. At low temperatures, the path essentially follows three straight line segments, along the lower border, across the plane, and finally along the upper border, thus avoiding extra steps of the CIM potential at $N = 1$ and $N = 3$. As the temperature increases, the path becomes smoother and passes through the $N = 1$ and $N = 3$ steps of the CIM potential, leading to the extra steps in the evolution of the densities at higher temperature. While for low temperatures the agreement of the DFT results with the exact ones is excellent, at higher temperatures deviations appear. Although DFT qualitatively captures the appearance of the extra steps in the evolution of the density versus gate voltage, their heights are not correctly reproduced in DFT. Presumably, this discrepancy can be attributed to the development of a δN dependence of the CIM potential at finite temperature, and will be addressed in future work.

Finally, we turn our attention to regimes II and III, which are both characterized by the appearance of the peculiar skew term in the Hxc potential. Figure 9(a) directly compares the evolution of the density as a function of the gate in both regimes. As we can see, the behavior is actually quite similar for both regimes, and not so different from regime I (cf. Fig. 8): As the gate increases, first the orbital with the higher interaction (here U_2) becomes half filled, and then the orbital with the lower interaction (U_1). Then upon further increase
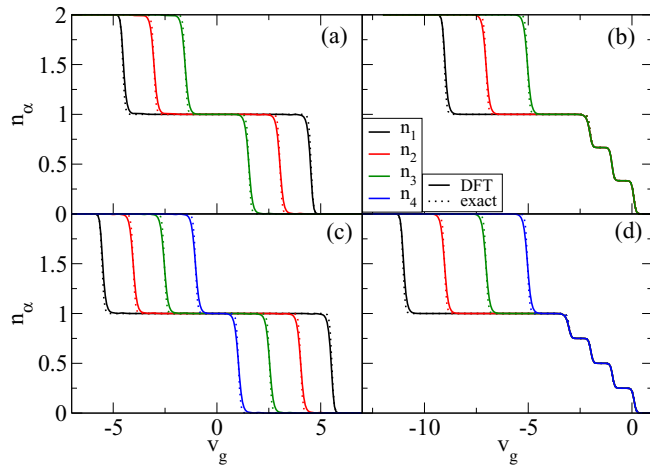
FIG. 10. Local occupations for the triple (a), (b) and quadruple (c), (d) QDs as function of the gate voltage. In the left panels, the QD levels are taken at particle hole ($v_\alpha = \epsilon_\alpha^* + v_g$) and in the right the impurity level is set to zero ($v_\alpha = v_g$). $\beta = 20/U'$ and $U_1 = 5U'$, $U_2 = 4U'$, $U_3 = 3U'$, $U_4 = 2U'$. All energies in units of U'.

of the gate, the order of emptying is reversed. Due to the higher interorbital interaction in regime III, the width of the central plateau is increased for both orbitals. Again, at low temperature the agreement with the exact results is excellent, but at higher temperatures moderate quantitative deviations occur (not shown).

To investigate the influence of the skew term in the Hxc potential on the evolution of the densities, we next concentrate on regime II and explore different paths in the $n_1 - n_2$ plane. To this end, we fix the energy splitting $\delta v = v_1 - v_2$ between the orbitals to different values while the total gate changes, i.e., $v_1 = \delta v + v_g$ and $v_2 = v_g$. Figure 9(b) shows the evolution of the density for two different values of δv and, correspondingly, different paths in the $n_1 - n_2$ plane (shown in the inset). For $\delta v = 0$, we observe an interesting effect. As the gate increases, the occupation of orbital 2 decreases in two steps, first to half filled and then further to zero, while the first orbital remains fully occupied. Then, around $v_g = -1$, the occupation of orbital 1 decreases abruptly to quarter filling, while now the occupation of orbital 2 increases again to quarter filling, $n_1 = n_2 = \sim 0.5$. This nonmonotonic behavior of the occupation of orbital 2 is reminiscent of the so-called level occupation switching (LOS) [56,57]. We find similar behavior in regime III (not shown).

B. Results for more than two orbitals

Finally, we apply the generalization of the Hxc potential Eq. (18) for more than two orbitals to DFT calculations of multiorbital QDs. Figure 10 shows the evolution of the density **n** as a function of the applied gate voltage v_g for three- [Figs. 10(a) and 10(b)] and four-level [Figs. 10(c) and 10(d)] QDs with all intraorbital Coulomb repulsions U_α different and constant interdot repulsion $U'(U_1 > U_2 > \ldots > U')$ at low temperature. In Figs. 10(a) and 10(c), the gate v_g is applied with respect to the phs point, i.e., $\epsilon_\alpha^* = -\frac{U_\alpha}{2} - \sum_{\beta \neq \alpha} U_{\alpha\beta}$. In this case, the path in the three- or four-dimensional density space avoids the steps in the CIM Hxc potential away from

half filling ($N = \mathcal{M}$), resulting in only three plateaus in the density evolution with the gate, in a similar way as in the DQD [cf. Fig. 8(a)]. On the other hand, in Figs. 10(b) and 10(d) (where $\epsilon_\alpha = 0$ and thus $\delta v_{\alpha\beta} = 0$), two (three) extra steps related to the interorbital Coulomb repulsions appear in the triple (quadruple) QD. The agreement between the DFT and the exact results is remarkable in all cases, showing that the generalization of Eq. (18) of the Hxc potential to more than two orbitals is valid. Finding similar expressions for a more general choice of parameters will be the focus of future work.

VI. CONCLUSIONS

In this paper, we have obtained Hxc potentials for DQDs in the grand-canonical ensemble subject to generic density-density interactions and Hund's rule coupling by reverse engineering from exact many-body solutions. The structure of the Hxc potentials consists of ubiquitous steps whose exact positions depend on the regime defined by the interaction parameters. This structure can be understood and derived from an analysis of the stability diagrams. In a second step, we were able to rationalize the step structure of the Hxc potential by a decomposition of the interaction into basic components. This decomposition allows us to write the Hxc potential of the system as a sum over basic Hxc potentials, which can be parametrized in a straightforward manner. Importantly, the decomposition into basic potentials can be generalized to multiorbital systems with more than two orbitals. DFT calculations employing the thus parametrized Hxc potentials for double, triple, and quadruple QDs show excellent agreement with exact results at low temperatures. At higher temperatures, we find moderate quantitative deviations from the exact results that we attribute to the modulation of step widths for finite $\delta n = n_1 - n_2$ not captured in our parametrization.

The parametrization of the Hxc potential derived here could be directly applied, e.g., to the description of single atoms where density-density and Hund's coupling are the dominating terms of the Coulomb interaction. Possible further applications regard the description of transport through multiorbital QDs or molecules coupled to leads. Due to the similarity between broadening by finite temperature, on the one hand, and finite coupling to the leads on the other hand, we expect that the Hxc potentials for finite coupling to the leads have a similar structure to the ones discussed here [58]. One way to incorporate finite coupling to the leads in the Hxc potential is by introduction of an effective temperature [59]. For the description of nonequilibrium effects, the i-DFT framework may be employed which in addition to the Hxc gate potential requires a parametrization of the xc bias [50]. This would also allow one to compute many-body spectral functions of interacting multiorbital systems [60].

[1] P. Hohenberg and W. Kohn, Phys. Rev **136**, B864 (1964).
[2] W. Kohn and L. J. Sham, Phys. Rev. **140**, A1133 (1965).
[3] R. M. Dreizler and E. K. U. Gross, *Density Functional Theory* (Springer, Berlin, 1990).
[4] J. P. Perdew, Phys. Rev. Lett. **55**, 1665 (1985).
[5] A. D. Becke, Phys. Rev. A **38**, 3098 (1988).
[6] J. P. Perdew, K. Burke, and M. Ernzerhof, Phys. Rev. Lett. **77**, 3865 (1996); **78**, 1396(E) (1997).
[7] J. P. Perdew, A. Ruzsinszky, G. I. Csonka, O. A. Vydrov, G. E. Scuseria, L. A. Constantin, X. Zhou, and K. Burke, Phys. Rev. Lett. **100**, 136406 (2008).
[8] A. D. Becke, J. Chem. Phys. **98**, 5648 (1993).
[9] J. Heyd, G. Scuseria, and M. Ernzerhof, J. Chem. Phys. **118**, 8207 (2003).
[10] J. P. Perdew, R. G. Parr, M. Levy, and J. L. Balduz, Phys. Rev. Lett. **49**, 1691 (1982).
[11] E. Sagvolden and J. P. Perdew, Phys. Rev. A **77**, 012517 (2008).
[12] P. Gori-Giorgi and A. Savin, Int. J. Quantum Chem. **109**, 2410 (2009).
[13] L. J. Sham and M. Schlüter, Phys. Rev. B **32**, 3883 (1985).
[14] P. W. Anderson, Phys. Rev. **124**, 41 (1961).
[15] J. Hubbard, Proc. R. Soc. Lond. A **276**, 238 (1963).
[16] A. Georges, G. Kotliar, W. Krauth, and M. J. Rozenberg, Rev. Mod. Phys. **68**, 13 (1996).
[17] G. Kotliar, S. Y. Savrasov, K. Haule, V. S. Oudovenko, O. Parcollet, and C. A. Marianetti, Rev. Mod. Phys. **78**, 865 (2006).
[18] D. Jacob, K. Haule, and G. Kotliar, Phys. Rev. B **82**, 195115 (2010).
[19] C. Weber, D. J. Cole, D. D. O'Regan, and M. C. Payne, Proc. Nat. Acad. Sci. USA **111**, 5790 (2014).
[20] M. Karolak, G. Ulm, T. O. Wehling, V. Mazurenko, A. Poteryaev, and A. Lichtenstein, J. Electron Spectrosc. Relat. Phenom. **181**, 11 (2010).
[21] R. Requist and E. K. U. Gross, Phys. Rev. B **99**, 125114 (2019).
[22] J. P. Coe, Phys. Rev. B **99**, 165118 (2019).
[23] L. Mazouin, M. Saubanère, and E. Fromager, Phys. Rev. B **100**, 195104 (2019).
[24] K. Haule, Phys. Rev. Lett. **115**, 196403 (2015).
[25] O. Gunnarsson and K. Schönhammer, Phys. Rev. Lett. **56**, 1968 (1986).
[26] K. Schönhammer, O. Gunnarsson, and R. M. Noack, Phys. Rev. B **52**, 2504 (1995).
[27] N. A. Lima, L. N. Oliveira, and K. Capelle, Europhys. Lett. **60**, 601 (2002).
[28] N. A. Lima, M. F. Silva, L. N. Oliveira, and K. Capelle, Phys. Rev. Lett. **90**, 146402 (2003).
[29] R. López-Sandoval and G. M. Pastor, Phys. Rev. B **67**, 035115 (2003).
[30] G. Xianlong, M. Polini, B. Tanatar, and M. P. Tosi, Phys. Rev. B **73**, 161103(R) (2006).
[31] K. Capelle and V. L. Campo Jr., Phys. Rep. **528**, 91 (2013).
[32] V. Brosco, Z.-J. Ying, and J. Lorenzana, Sci. Rep. **3**, 2172 (2013).
[33] Z.-J. Ying, V. Brosco, and J. Lorenzana, Phys. Rev. B **89**, 205130 (2014).
[34] D. Carrascal, J. Ferrer, J. Smith, and K. Burke, J. Phys.: Condens. Matter **29**, 019501 (2015).
[35] T. Müller, W. Töws, and G. M. Pastor, Computation **7**, 66 (2019).
[36] C. Verdozzi, G. Stefanucci, and C.-O. Almbladh, Phys. Rev. Lett. **97**, 046603 (2006).
[37] C. Verdozzi, Phys. Rev. Lett. **101**, 166401 (2008).
[38] S. Kurth, G. Stefanucci, E. Khosravi, C. Verdozzi, and E. K. U. Gross, Phys. Rev. Lett. **104**, 236801 (2010).
[39] J. I. Fuks and N. T. Maitra, Phys. Rev. A **89**, 062502 (2014).
[40] J. I. Fuks and N. T. Maitra, Phys. Chem. Chem. Phys. **16**, 14504 (2014).
[41] N. Dittmann, J. Splettstoesser, and N. Helbig, Phys. Rev. Lett. **120**, 157701 (2018).
[42] N. Dittmann, N. Helbig, and D. M. Kennes, Phys. Rev. B **99**, 075417 (2019).
[43] G. Stefanucci and S. Kurth, Phys. Rev. Lett. **107**, 216401 (2011).
[44] J. P. Bergfield, Z.-F. Liu, K. Burke, and C. A. Stafford, Phys. Rev. Lett. **108**, 066801 (2012).
[45] P. Tröster, P. Schmitteckert, and F. Evers, Phys. Rev. B **85**, 115409 (2012).
[46] A. Georges, L. de' Medici, and J. Mravlje, Ann. Rev. Condens. Matter Phys. **4**, 137 (2012).
[47] M. Seidl, J. P. Perdew, and M. Levy, Phys. Rev. A **59**, 51 (1999).
[48] A. Mirtschink, M. Seidl, and P. Gori-Giorgi, Phys. Rev. Lett. **111**, 126402 (2013).
[49] N. Mermin, Phys. Rev. **137**, A1441 (1965).
[50] G. Stefanucci and S. Kurth, Nano Lett. **15**, 8020 (2015).
[51] G. Stefanucci and S. Kurth, Phys. Stat. Sol. (b) **250**, 2378 (2013).
[52] S. Kurth and G. Stefanucci, J. Phys.: Condens. Matter **29**, 413002 (2017).
[53] T. Dimitrov, H. Appel, J. Fuks, and A. Rubio, New J. Phys. **18**, 083004 (2016).
[54] E. Perfetto and G. Stefanucci, Phys. Rev. B **86**, 081409(R) (2012).
[55] G. Xianlong, A-Hai Chen, I. V. Tokatly, and S. Kurth, Phys. Rev. B **86**, 235139 (2012).
[56] P. G. Silvestrov and Y. Imry, New J. Phys. **9**, 125 (2007).
[57] Y. Kleeorin and Y. Meir, Phys. Rev. B **96**, 045118 (2017).
[58] S. Kurth and G. Stefanucci, Phys. Rev. B **94**, 241103(R) (2016).
[59] N. Sobrino, R. D'Agosta, and S. Kurth, Phys. Rev. B **100**, 195142 (2019).
[60] D. Jacob and S. Kurth, Nano Lett. **18**, 2086 (2018).